A Mathematical Model for Determining an Electrohydrodynamic Accelerator's Monopolar Flow Limit During Positive Corona Discharge

Emmanouil D. Fylladitakis, Antonios X. Moronis, and Michael P. Theodoridis

***Abstract*— This paper presents a mathematical model establishing the velocity limit of electrohydrodynamics fluid accelerators with tip to plane and cylinder to plane electrode configurations. The model is based on the calculation of the electric field lines length and trajectory, allowing practical use even if only the spatial characteristics of the geometry, the fluid's ion mobility and the applied voltage are known. Experiments are performed with wire-plane and needle-grid electrode configurations to validate the developed mathematical model, both for the calculation of the average flow limit of the geometry and for the calculation of the flow limit at the end of each electric field line.**

***Index Terms*— Corona discharge, electrohydrodynamics (EHD), electrokinetics, electrostatic fluid accelerator (EFA).**

I. Introduction

ELECTROHYDRODYNAMIC (EHD) flow is known to occur between two asymmetric high-voltage electrodes during corona discharge. As the charged particles move between the electrodes, they collide with the inert particles of the fluid, transferring their momentum and thus creating a bulk flow, known as "ionic wind." The phenomenon was first observed in the seventeenth century, but scientists were unable to explain the phenomenon [1], [2]. The first quantitative studies were performed nearly two centuries later by Chattock [3], whose work was extended by E. Lob in 1954 [4].

Due to the complexity of the phenomenon, there have been few studies analyzing ionic wind mechanisms in the twentieth century [5], [6]. However, modern research methods and numerous trending EHD engineering applications have greatly increased the research interest during the past two decades [7]. Still, the vast majority of the published research was focused on either simulated studies or the presentation of experimental results for specific applications, with the few mathematical models based on empirical approaches [8]–[13]. The first empirical expression of the EHD flow velocity limit was derived in [5] and later expanded in [14]. Robinson's model remains valid today but requires the calculation of the "geometrical factor," a constant that needs to be assessed via experimentation.

Corona discharge requires the use of electrodes with sufficiently small curvature radius, so as to generate a strong electric field capable of ionizing some of the fluid's molecules. From literature, it can be seen that the vast majority of practical applications rely on wire-plane or pin-plane configurations, as the small curvature of the emitter creates a strong inhomogeneous electric field with excellent corona discharge results [7].

This paper presents a mathematical model establishing the velocity limit of EHD fluid accelerators with tip-plane, sphere-plane, and cylinder-plane electrode configurations. The proposed model is based on the exact calculation of the electric field lines and can be easily utilized if only the spatial characteristics of the geometry, the fluid's ion mobility and the applied voltage are known. It should be noted that the proposed model assumes there is no effect on the length and/or formation of the field line by space charges, or that the effect is insignificant. Although an approximation, this approach is considered to be acceptable for the estimation of real-world applications, as the difference between Laplacian electric field lines and those obtained from more complex models is not significant [15]. We experimentally verify the model for needle-grid and wire-plane configurations, as well as with the published results of previously published experimental studies of other researchers. Positive coronas have only been examined due to the fact that they are more stable and efficient for most applications [16], [17].

II. Methodology

It is known that the ionic wind is the result of charged ions colliding with neutral air molecules and atoms as they traverse the electric field lines, transferring their momentum via collisions. Although the ions will be neutralized once they reach the collector electrode, the neutral particles will continue their movement. Therefore, the EHD velocity limit can be

Manuscript received September 13, 2016; revised January 12, 2017; accepted January 31, 2017. Date of publication February 14, 2017; date of current version March 8, 2017.

E. D. Fylladitakis is with the Department of Electronics and Computer Engineering, Brunel University London, London, U.K., and also with the Department of Energy Technology Engineering, Technological Educational Institute of Athens, Athens, Greece (e-mail: emm.fyll@gmail.com).

A. X. Moronis is with the Department of Energy Technology Engineering, Technological Educational Institute of Athens, Athens 12210, Greece (e-mail: amoronis@teiath.gr).

M. Theodoridis is with the Department of Electronics and Computer Engineering, Brunel University London UB8 3PH, London, U.K. (e-mail: michael.theodoridis@brunel.ac.uk).

Color versions of one or more of the figures in this paper are available online at http://ieeexplore.ieee.org.

Digital Object Identifier 10.1109/TPS.2017.2663778

calculated via the space charge density distribution. This method was initially proposed by Sigmond, who simplified the model by using approximates for the electric field lines and field intensity [15]. The exact trajectory and length of the electric field lines is required for an analytical solution based on this theory. Therefore, the mathematical solution for the precise calculation of the field lines emanating from electrodes with a cylindrical or spherical surface is presented.

A. Space Charge Distribution Model

Considering each field line emerging from a sharp corona electrode and ending at the collecting electrode's surface, we get the trajectories of charged particles moving under the electric field force. The drifting charged particles transfer their momentum to the neutral particles via collisions taking place along their drift path, resulting to a flow velocity proportional to the velocity of the charged particles. Assuming that the unipolar current density limit at the ending point of each field line is j_S, then we can calculate the EHD velocity limit v_S by applying (1) [12], [14], [18], [19]

$$v_S = \sqrt{\frac{j_S L}{\rho \mu}} \frac{\text{m}}{\text{s}} \tag{1}$$

where L is the total length of the field line, ρ is the density of air with $\rho = 1.29$ kg/m^3 and μ is the average ion mobility in air, which is usually considered to be within the range from 1.8 to 2.2 $\times$ 10^{-4}m^2/ (Vs) [20]–[23].

Semi-analytical studies have been published for wire-plane and point-plane geometries, where the equations governing the charged species were formulated along the field lines. In these studies, the corona current distribution was based on the well-known Deutsch's approximation model and the results were compared to finite element model simulations [24]–[26]. However, the unipolar current flow limit at the impact point of each field line can be expressed in relation to the length of the field line and is given by (2) [15], [27]

$$j_s = \mu \varepsilon_0 \frac{V^2}{L^3} \frac{\text{A}}{\text{m}^2}. \tag{2}$$

Therefore, if the length of the electric field lines is known, the unipolar current flow limit and, in extend, the EHD velocity limit can be mathematically assessed.

B. Field Lines Model

According to bibliography, the field lines in a cylinder-plane electrode configuration are circular arcs emerging from, or impinging to the electrodes at right angles. The sole exception is the shortest field line emerging from the lower center point on the cylinder's surface facing the plane, which decays into a straight line crossing the gap d. These arcs are centered on the plane electrode, as shown in Fig. 1, where the geometric arrangement of the electrodes is illustrated. Note that, according to the well-known method of image charges for the calculation of electric fields, the additional cylinder at the left represents the "image" electrode [28].

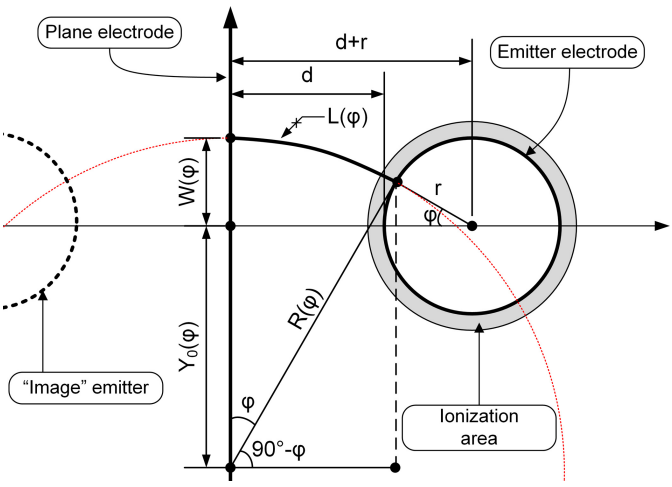

Fig. 1. Cylinder-plane electrode configuration and the formation of field lines.

As seen in Fig. 1, the field lines emanated from an emission angle φ have an arc length of

$$L(\varphi) = \varphi R(\varphi). \tag{3}$$

The distance $Y_0(\varphi)$ to the center of each field line's arc is

$$Y_0(\varphi) = R(\varphi)\cos(\varphi) - r\sin(\varphi). \tag{4}$$

According to Fig. 1, $R(\varphi)$ can be given by the expression

$$R(\varphi) = \frac{(d+r) - r\cos(\varphi)}{\sin(\varphi)}. \tag{5}$$

The combination of (4) and (5) gives the solution for the distance Y_0

$$Y_0(\varphi) = (d+r)\cot(\varphi) - \text{rcsc}(\varphi). \tag{6}$$

Referring to Fig. 1, it can also be shown that each field line impinges on the plane electrode at distance $W(\varphi)$ from the cylinder's axis X, where

$$W(\varphi) = R(\varphi) - Y_0(\varphi) = (d+2r)\tan\left(\frac{\varphi}{2}\right). \tag{7}$$

Using the above equations, it is easy to calculate the length and trajectory of each field line, as well as the distance of its impact point on the plane electrode from the axis of symmetry. Fig. 2(a) illustrates the formation of three field lines for $V = 1$ kV, $d = 5$ cm and $r = 0.5$ cm at different φ angles, ranging from 0° to 90°, in 30° steps, for a wire-plane configuration. It should be noted that the model remains valid for geometries where the collector electrode is a grid instead of a plane, assuming that the grid is relatively dense, as it will not affect the length of the field lines or the strength of the electric field significantly. The model introduced in this section could also be applied in the case of a tip-plane electrode configuration, assuming a tip with hemi-spherical shape. In this case, the shape of the field lines remains practically the same (circular arcs), despite the transition from longitudinal to spherical symmetry [Fig. 2(b)].

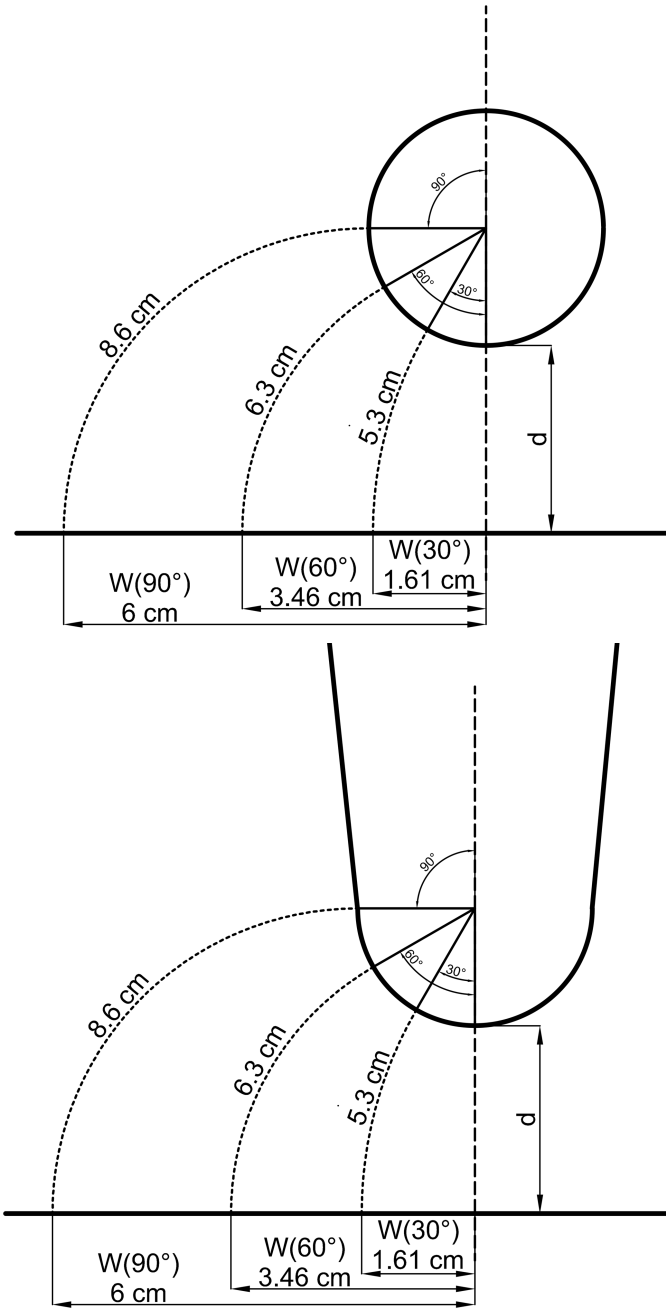

Fig. 2. Field lines formation for $V = 1$ kV, $d = 5$ cm and $r = 0.5$ cm in 30° steps, up to 90°, for a wire-plane configuration (top) and for a tip-plane configuration (bottom).

III. Experimental Setup

A. Wire-Plane Electrode Setup

In order to verify the validity of the developed mathematical models, experiments were performed using various wire-plane and needle-grid configurations. The wire-plane setup has been used to verify the application of (1) for the assessment of the maximum velocity limit. By substituting j_s from (2) into (1), it can be seen that the maximum velocity will appear at the end of the shortest field line, which is emanated from $\varphi = 0°$ and is a straight line across the gap d. On that purpose, Ni–Cr wires of appropriate diameter were used as emitters above a flat plane collector electrode, which had a pitot tube inserted beneath it. The length of the emitter and collector electrodes was 30 cm, while the width of the plane collector is 58 cm. A basic schematic of the experimental setup is given in Fig. 3.

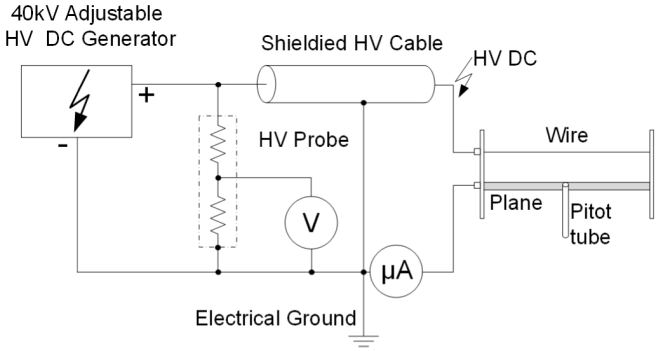

Fig. 3. Experimental setup.

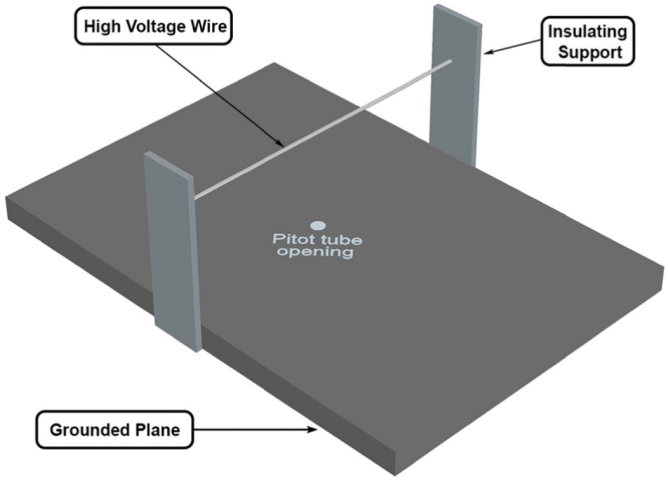

Fig. 4. Indicative 3-D illustration of the wire-plane electrode configuration.

The required high voltage was supplied by an adjustable high voltage power source (Matsusada Precision W Series). A voltmeter combined with a Coline HV40B 40 kV 1000:1 high-voltage probe were used for measuring the dc high voltage applied to the emitter electrode, with an accuracy of 1%. Current readings (corona current) have been acquired by a high precision ammeter with 1 nA sensitivity. The Pitot manometer is an Extech HD350 and the anemometer is an Extech AN200. All the experiments were performed in atmospheric air, with temperature ranging from 25 °C to 27 °C, and relative humidity between 45% and 52 %.

An opening of 2.6 mm, exactly the radius of the tube's point, was drilled on the surface of the plane electrode directly beneath the emitter wire. Fig. 4 displays an indicative 3-D illustration of the wire-plane geometry.

B. Tip-Plane Electrode Setup

For the estimation of the average EHD velocity limit, a needle-grid configuration was used. The setup is inserted into a cylindrical tube that forms the boundaries of both the

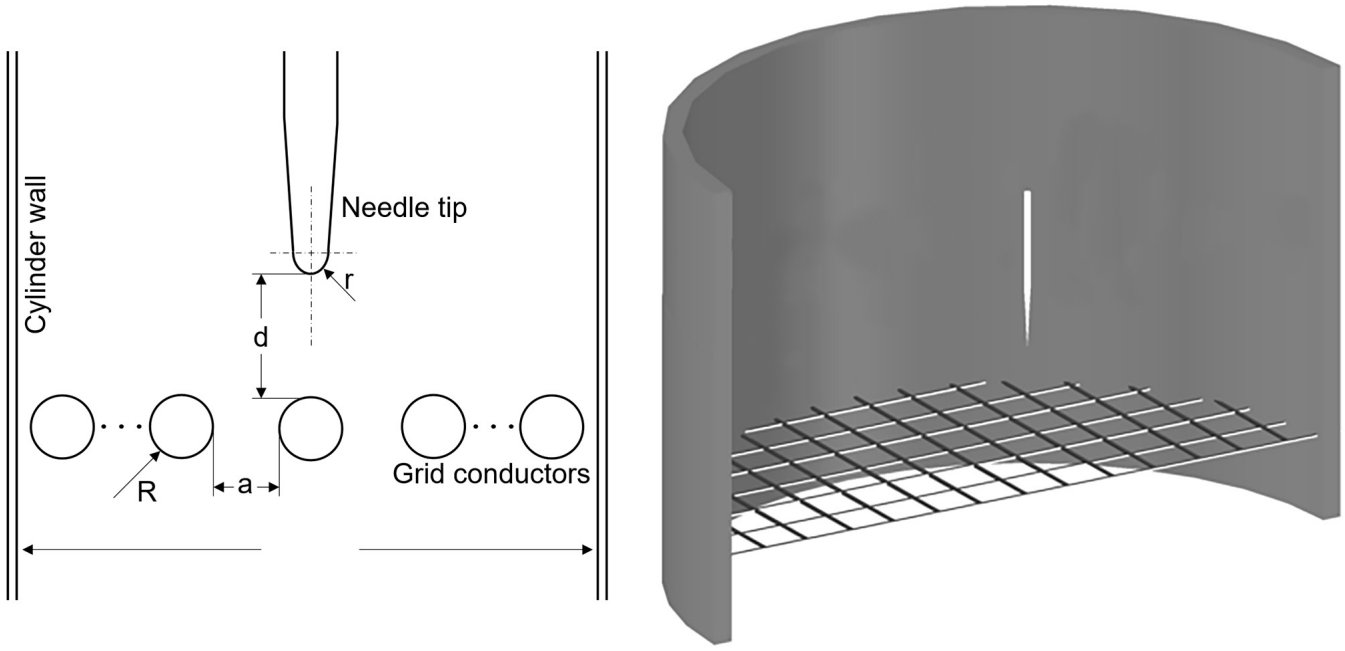

Fig. 5. Indicative 2-D schematic and 3-D illustration of the needle-grid electrode configuration.

mathematical and experimental assessment, simplifying the problem. An anemometer is attached at the exit of the tube, three centimetres after the grid, measuring the wind velocity of the EHD setup. The experimental tube has been selected to be of exactly the same diameter as the anemometer's rotary sensor (74 mm). A single steel needle with a tip radius $r = 32\ \mu$m is used as an emitter and a steel grid with wire radius $R = 520\ \mu$m and a nominal aperture of 66% is used as a collector. Fig. 5 displays an indicative 2-D schematic and a 3-D illustration of the needle-grid geometry.

When the distance d between the electrodes is much greater than the radius R and aperture a of the grid electrode, the grid can be assumed to be closely resembling a plane [29].

IV. Results and Discussion

A. Wire-Plane Electrode Setup

The wire-plane setup is used to verify the application of (1) for the assessment of the maximum velocity limit. The theoretical approach is based on the assumption of unipolar current flow and it is only natural that the calculated EHD velocity limit will be aligned with the unipolar saturation current flow limit. Fig. 6 displays a graphical representation of the wire-plane geometry, showing the formation of the electric field lines.

According to (2), the maximum current density $j_{s_{\max}}$ will appear at the end of the shortest field line $L_{\min}$, which is a straight line emanating from $\varphi = 0°$ and crossing the gap with $L_{\min} = d$. Then, it can be shown from (1) that the corresponding velocity also becomes maximum. So the maximum velocity limit $v_{w_{\max}}$ of the geometry would be

$$v_{w_{\max}} = \sqrt{\frac{j_{s_{\max}} d}{\rho \mu}} = \sqrt{\frac{\varepsilon_0 V^2}{\rho d^2}} \frac{\text{m}}{\text{s}}. \tag{8}$$

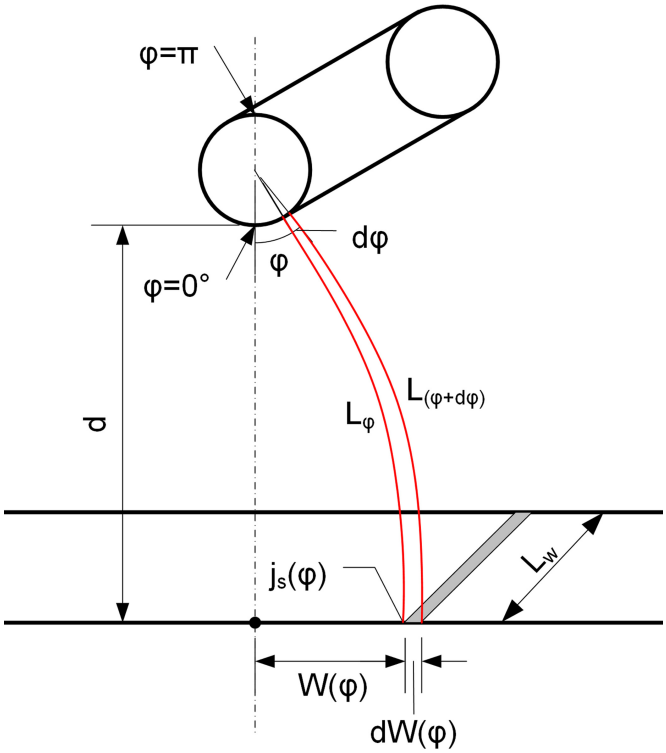

Fig. 6. Indicative schematic of the field lines formation with a wire-plane electrode configuration.

According to (2), the current on a stripe of width $dW(\varphi)$ would then be

$$dI_{\text{sw}-p} = dW(\varphi) L_w j_s(\varphi) \text{A} \tag{9}$$

where the width $dW(\varphi)$ is

$$dW(\varphi) = \frac{d+2r}{1+\cos(\varphi)} d\varphi \text{m}. \tag{10}$$

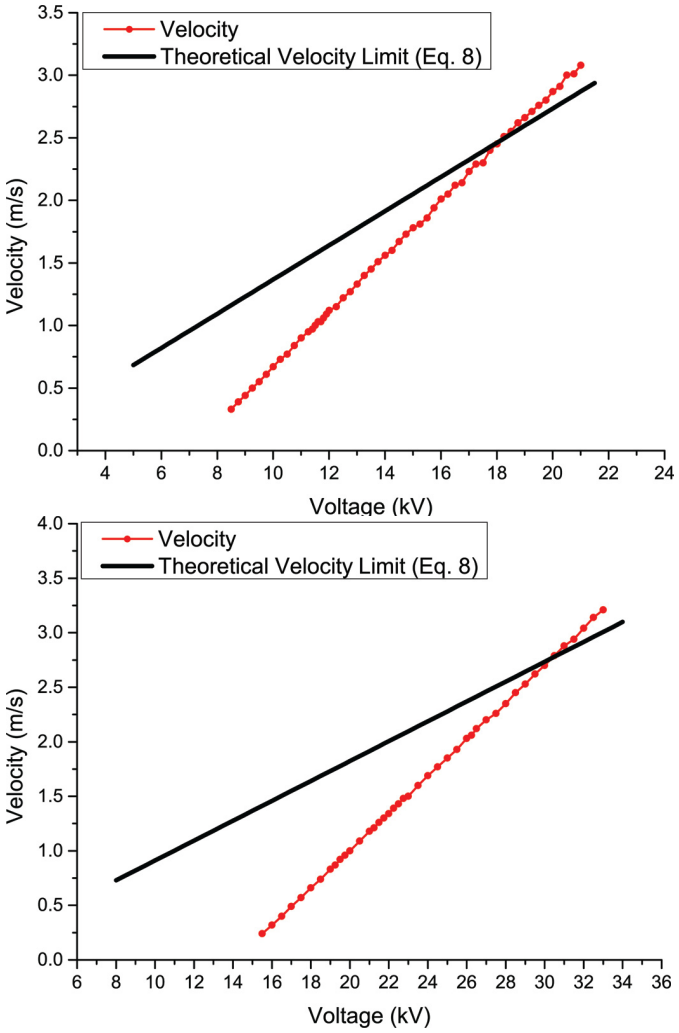

Fig. 7. Correlation between the measured maximum velocity and the calculated velocity limit of a wire-plane configuration according to (8) for $d = 2$ cm, $r = 40$ μm (top) and $d = 3$ cm, $r = 140$ μm (bottom).

Therefore, for the entire wire-plane electrode geometry, the total unipolar saturation current can be found by the integral $I_{\mathrm{sw}-p} = \int dI_{\mathrm{sw}-p}$ over the whole current flow space. By substituting $dI_{\mathrm{sw}-p}$ from (9) and (10), an integral over $d\varphi$ is derived, where the integral limits are defined by the geometry

$$I_{\mathrm{sw}-p} = 2\int_0^{\pi} \frac{d+2r}{1+\cos(\varphi)} L_w j_s(\varphi) d\varphi \mathrm{A}. \tag{11}$$

Note that the integral of (11) is multiplied by two in order to bilaterally cover the geometry in relation to the center of the emitter electrode. Figs. 7 and 8 display the correlation between the unipolar saturation current and the EHD velocity limit for various geometries. The average ion mobility in air is considered to be $1.8 \times 10^{-4}\mathrm{m}^2/(\mathrm{Vs})$. It can be seen that the corona current tends to approach and or slightly exceed the saturation current limit near the breakdown point of the electrode setup. The gradually diminishing difference between the experimental velocity and the theoretical velocity limit at higher voltage levels displays the expected development of the phenomenon, as the ionic drift region outside the ionization region acts as an impedance and is what gives the corona discharge its characteristic intrinsic stability [30].

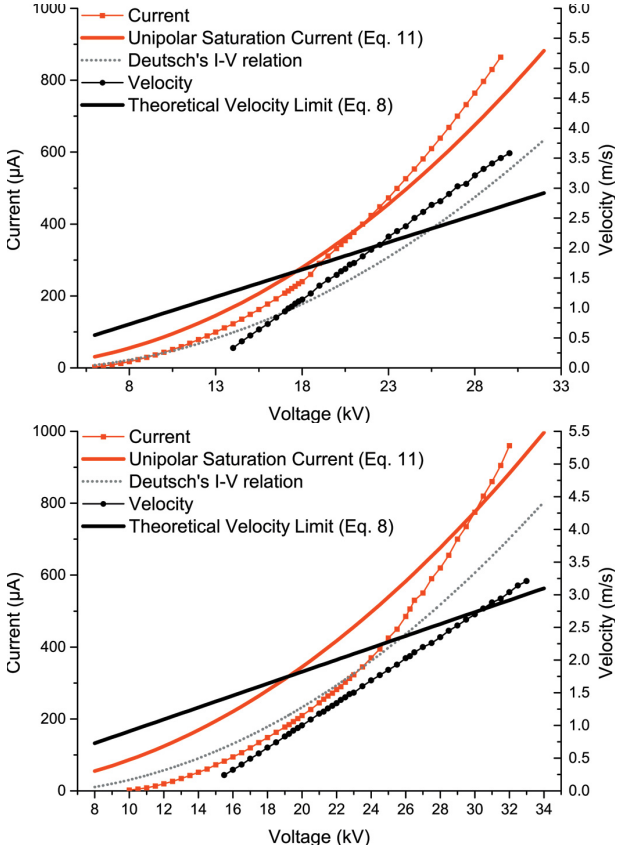

Fig. 8. Correlation between the corona current and the EHD velocity of a wire-plane configuration according to (8) for $d = 3$ cm, $r = 40$ μm (top) and $d = 3$ cm, $r = 140$ μm (bottom).

Figs. 8–10 show that the voltage levels at which the measured current crosses the corresponding unipolar saturation current limit, or the measured air velocity crosses the theoretical velocity limit, are very near or coincide.

Once the unipolar saturation current limit has been surpassed, it is a clear indication that bipolar conduction phenomena are emerging, such as streamers, resulting in currents higher than the anticipated unipolar conduction limit [27]. These phenomena, however, do not seem contribute to the EHD velocity.

As it can be seen in Fig. 10, from a highly asymmetric configuration that strongly favors the formation of bipolar conduction, the EHD velocity continues to increase linearly even after the unipolar saturation current limit has been reached, even though the current is growing exponentially. We can also notice that the calculations based on Deutsch's relation [25], [26] tend to significantly underestimate the current for geometries with highly asymmetric electric fields and, should they have been used instead of the proposed current distribution model, would also significantly underestimate the velocity. Finally, assuming that the gap d is much greater than the emitter electrode radius r, then (2) and (10) can be reduced to

$$j_s'(\varphi) = \mu\varepsilon_0 V^2 \left(\frac{\sin(\varphi)}{\varphi}\right)^3 \frac{1}{d^3}\frac{\mathrm{A}}{\mathrm{m}^2} \tag{12}$$

$$dW'(\varphi) = \frac{d}{1+\cos(\varphi)} d\varphi \mathrm{m}. \tag{13}$$

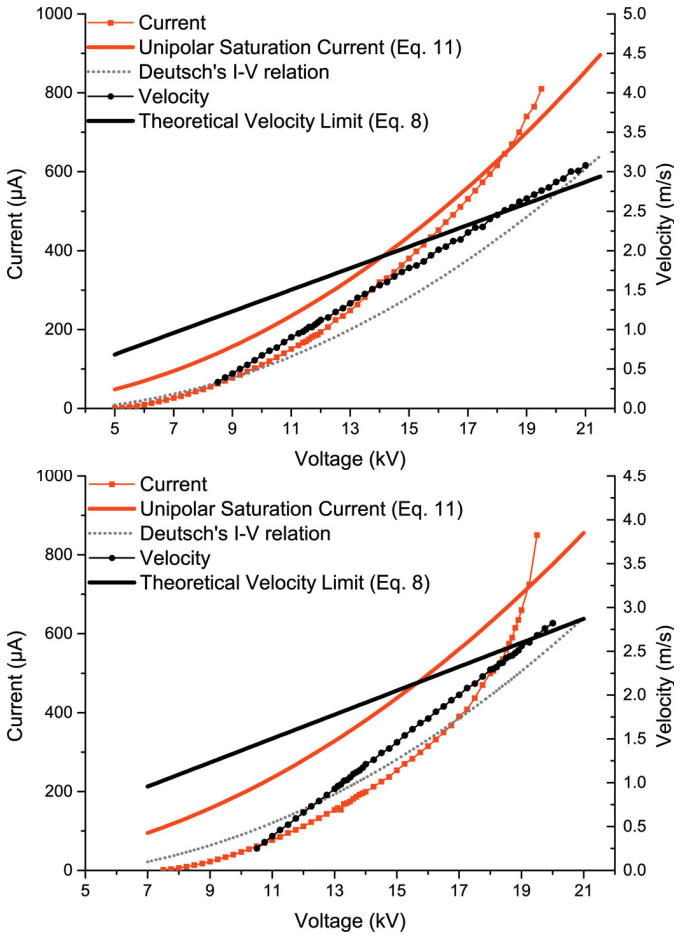

Fig. 9. Correlation between the corona current and the EHD velocity of a wire-plane configuration according to (8) for $d = 2$ cm, $r = 40$ μm (top) and $d = 2$ cm, $r = 100$ μm (bottom).

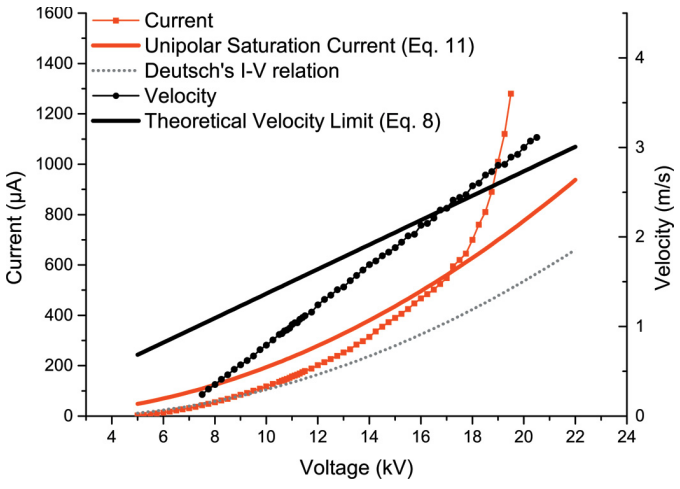

Fig. 10. Correlation between the corona current and the EHD velocity according to (8) for $d = 2$ cm, $r = 30$ μm.

Therefore, (11) can be greatly simplified

$$I'_{sc-p} = 1.62\frac{L\mu\varepsilon_0 V^2}{d^2}\text{A}. \tag{14}$$

B. Tip-Plane Electrode Setup

In this section we examine the output of the mathematical model using a needle-grid electrode configuration and researching the average velocity limit of the geometry. Fig. 11 shows the formation of the field lines for this geometry, which resembles a standard tip-plane electrode setup.

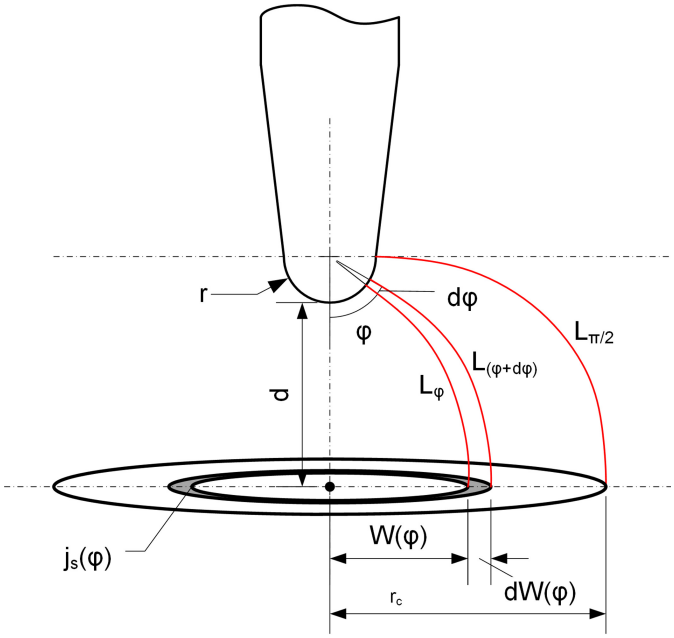

Fig. 11. Indicative schematic of the field lines formation with a tip-plane electrode configuration.

The current $dI_{\text{spt}-p}$ on the circular ring formed between the emanation angles φ and $\varphi + d\varphi$ is

$$dI_{\text{spt}-p} = \pi[(W(\varphi) + dW(\varphi))^2 - (W(\varphi))^2]j_s(\varphi)\text{A}. \tag{15}$$

In the case of a needle-grid geometry, (11) is adjusted to

$$I_{\text{st}-p} = \int_0^{\pi/2} 2\pi(d+2r)\tan\left(\frac{\varphi}{2}\right)\frac{d}{1+\cos(\varphi)}j_s(\varphi)d\varphi\text{A}. \tag{16}$$

Equation (15) shows the total current I_s up to the maximum emanation angle $\varphi_{\max}$ from the tip of the needle. As the tip of the needle resembles a hemisphere, this angle has a maximum of 90°. Furthermore, depending on the distance d between the electrodes and the radius r_c of the tube, the maximum angle may be limited to the angle that satisfies the condition $W(\varphi) = r_c$ to provide an approximate solution.

Similarly, the average velocity limit of the geometry could be found by integrating each field line's contribution over the plane and dividing the total by the plane's area

$$v_{t-p} = \frac{2}{r_c^2}\int_0^{\pi/2} W(\varphi)\text{d}W(\varphi)\sqrt{\frac{j_s(\varphi)L(\varphi)}{\rho\mu}}\frac{\text{m}}{\text{s}}. \tag{17}$$

This model is an approximation that ignores the contribution of the needle's body. However, considering that the bulk of the corona current flow comes from emission angles up to 90°, the results should be very close to those acquired via the experiments [15].

As it can be seen from Fig. 12, once again the EHD velocity is closely aligned with the unipolar current flow for

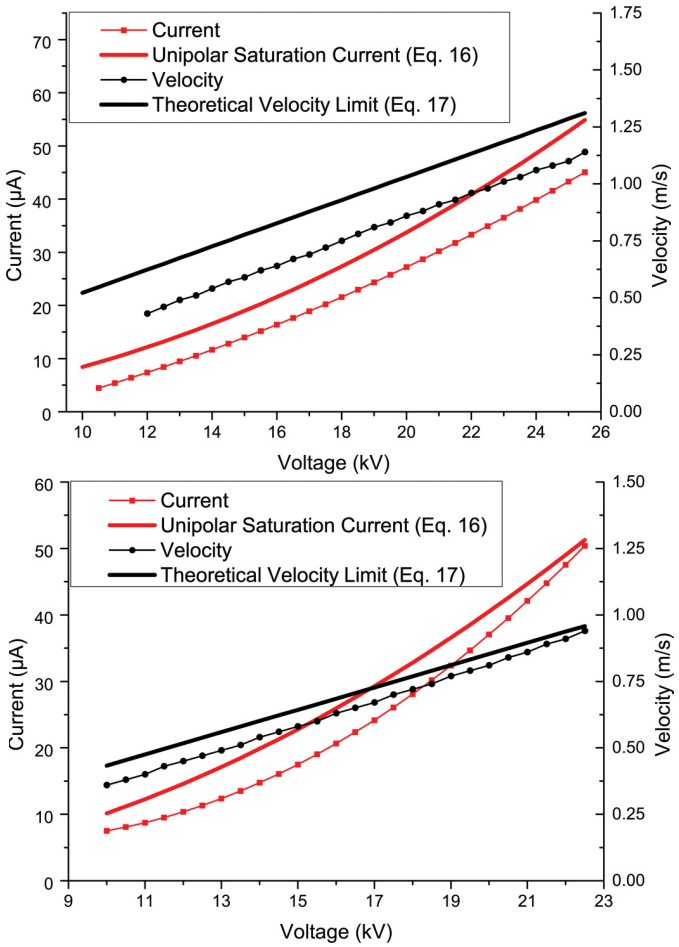

Fig. 12. Correlation between the corona current and the EHD velocity according to (17) for a needle-grid configuration of $r = 32\ \mu$m and $R = 520\ \mu$m, with an electrode gap d of 2.5 cm (top) and 3 cm (bottom).

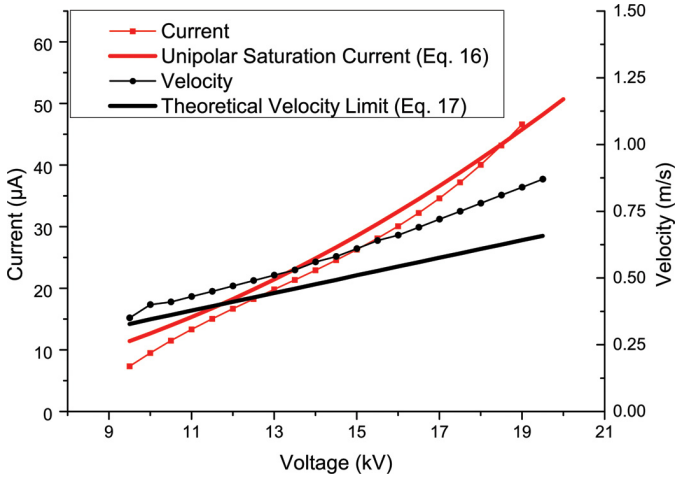

Fig. 13. Correlation between the corona current and the EHD velocity according to (17) for a needle-grid configuration of $d = 2$ cm, $r = 32\ \mu$m and $R = 520\ \mu$m.

a distance at least 50% greater than the discharge gap d. If the distance between the two electrodes is smaller, the electric field surrounding the needle's body can assist the acceleration of ions, particularly those emanating from large emission angles φ, resulting to velocities higher than anticipated (Fig. 13). It should also be noted that the type of grid

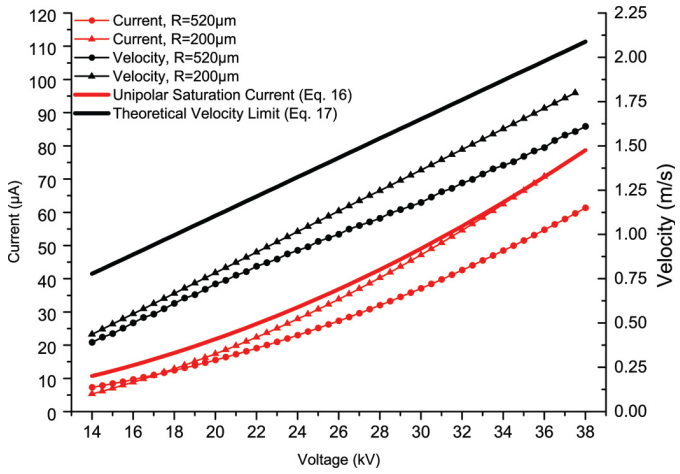

Fig. 14. Comparison of the EHD velocity and the corona discharge current according to (17) for needle-grid configurations using two different grid collectors ($d = 4$ cm, $r = 32\ \mu$m).

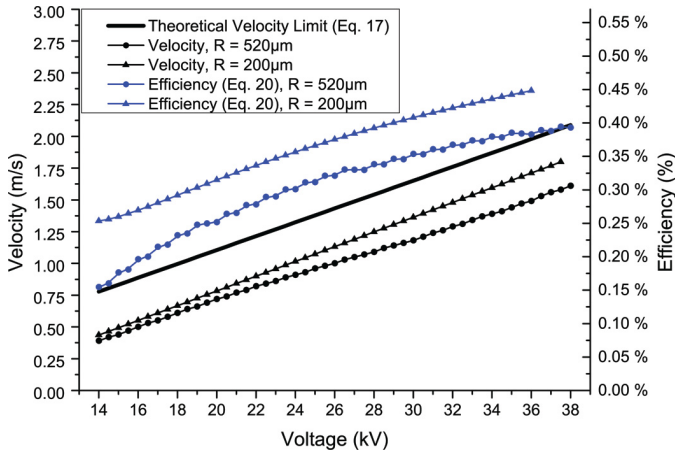

Fig. 15. Comparison of the EHD velocity and the efficiency for needle-grid configurations using two different grid collectors ($d = 4$ cm, $r = 32\ \mu$m).

affects both the formation of the electric field and the airflow impedance and, in extend, the EHD pump's velocity. As seen in Fig. 14, the use of a grid with wires of smaller radius ($R = 200\ \mu$m) and with greater nominal aperture (81%) significantly increases the corona current of the geometry. Even though the average air velocity increases, the difference is small compared to the increase of the current, especially considering the lower airflow impedance of the higher aperture grid.

As with the previous section, (14) and (15) can be greatly simplified if one assumes that the gap d is much greater than the emitter electrode radius r. By substituting (12) and (13) in (16), we get

$$I'_{\mathrm{st}-p} = \frac{\pi \mu \varepsilon_0 V^2}{2d} \mathrm{A}. \tag{18}$$

Similarly, (17) becomes

$$v'_{t-p} = 0.78 \frac{\mathrm{d}V}{r_c^2} \sqrt{\frac{\varepsilon_0}{\rho}} \frac{\mathrm{m}}{\mathrm{s}}. \tag{19}$$

C. Efficiency

The efficiency n of the apparatus (20) depends on the third power of the average air velocity and, thus, the use of the

higher aperture grid results to a higher energy conversion efficiency, despite the disproportional increase of the corona current (Fig. 15) [16]

$$n = \frac{\frac{1}{2}\rho\pi r_c^2 v_{\text{EHD}}^3}{V_{\text{in}} I_{\text{in}}} \times 100\% \tag{20}$$

where V_{in} and I_{in}, respectively are the input voltage and current of the EHD device.

V. Conclusion

This work presents a mathematical model assessing the velocity limit of EHD fluid accelerators. The model combines the known space charge distribution model with an analytical solution for the electric field lines for any electrode with a cylindrical or spherical surface facing a plane collector. As such, the model is usable even if only the spatial characteristics of the geometry, the fluid's ion mobility and the applied voltage are known. The model can also assess both the average velocity limit of the entire apparatus and the velocity limit at the endpoint of any electric field line. Do note that the developed models are based on the unipolar saturation current limit theory and display the maximum possible fluid velocity attainable assuming unipolar conduction. The voltage for which every geometry fully attains unipolar conduction depends on the asymmetry and strength of the developed electric field, i.e., on the geometrical characteristics of the geometry itself. Depending on the geometry, the corona current of the entire apparatus may be unable to reach the unipolar saturation current limit, such as when, for example, an emitter of high radius is placed at a short distance from a collector. The gap of such a configuration will go to breakdown long before the electric field can be strong enough to fully saturate the long field lines emanating from large emission angles.

As it is based on the same theory that indicates the unipolar saturation current limit, the velocity model is closely related to the unipolar discharge current of each geometry. Experimental testing using both wire-plane and needle-grid configurations has validated the results of the model and the link to the unipolar discharge current. The input current of the EHD device may not always produce the expected velocity output, especially if the device is operating within a range that produces extensive bipolar current conduction phenomena that do not assist the acceleration of the fluid. This has been experimentally verified as well, since geometries that develop large currents due to extensive bipolar phenomena display a disproportional rise to their input current after the unipolar saturation limit has been reached, while the fluid's velocity increases linearly. The voltage levels at which the measured current crosses the corresponding unipolar saturation current limit are near where the measured air velocity crosses the theoretical velocity limit as well, which was to be expected as the proposed velocity model is fundamentally based on the unipolar saturation current model. After that point however, the current displays a disproportional rise due to the extensive bipolar phenomena that do not assist the acceleration of the fluid, seriously impeding the efficiency of the device.

Experimental testing also revealed that the selection of a grid collector can be a complicated matter. Even though smaller grids can generate stronger electric fields that will promote the creation of bipolar conduction phenomena, raising the corona discharge current of the device, their smaller aperture can improve the energy conversion efficiency. The selection of the collector electrodes according to the application, fluid and expected output velocity is subject to fluid dynamics optimization studies.

References

[1] N. Cabeo, *Philosophia Magnetica*. Cologne, Germany: Francesco Suzzi, 1629.

[2] F. Hauksbee, *Physico-Mechanical Experiments on Various Subjects*. London U.K.: R. Brugis, 1709.

[3] A. P. Chattock, "On the velocity and mass of the ions in the electric wind in air," *Philos. Mag.*, vol. 48, no. 294, pp. 401–420, 1899.

[4] E. Lob, *Archiv der Elektrischen Uebertragun*. Stuttgart, Germany: Baden-Württemberg, 1954.

[5] M. Robinson, "Movement of air in the electric wind of the corona discharge," Hamon Research-Cottrell, Somerville, Somerville, NJ, USA, Tech. Rep. TP60-2, 1960.

[6] O. M. Stuetzer, "Magnetohydrodynamics and electrohydrodynamics," *Phys. Fluids*, vol. 5, no. 5, p. 534, 1962.

[7] E. D. Fylladitakis, M. P. Theodoridis, and A. X. Moronis, "Review on the history, research, and applications of electrohydrodynamics," *IEEE Trans. Plasma Sci.*, vol. 42, no. 1, pp. 358–375, Feb. 2014.

[8] D. J. Harney, "An aerodynamic study of the 'electric wind,'" Ph.D. dissertation, Dept. Eng. Appl. Sci. California Inst. Technol., Pasadena, Pasadena, CA, USA, 1957.

[9] A. Rashkovan, E. Sher, and H. Kalman, "Experimental optimization of an electric blower by corona wind," *Appl. Thermal Eng.*, vol. 22, pp. 1587–1599, Oct. 2002.

[10] M. Rickard, D. Dunn-Rankin, F. Weinberg, and F. Carleton, "Characterization of ionic wind velocity," *J. Electrostatics*, vol. 63, pp. 711–716, Jun. 2005.

[11] C. F. Chung and W. J. Li, "Experimental studies and parametric modeling of ionic flyers," in *Proc. IEEE/ASME Int. Conf. Adv. Intell. Mechatronics*, Sep. 2007, pp. 1–6.

[12] Y. Kitahara, K. Aoyagi, and R. Ohyama, "An experimental analysis of ionic wind velocity characteristics in a needle-plate electrode system by means of laser-induced phosphorescence," in *Proc. Annu. Rep.-Conf. Electr. Insul. Dielectr. Phenomena, (CEIDP)*, Oct. 2007, pp. 529–532.

[13] C. Kim, D. Park, K. C. Noh, and J. Hwang, "Velocity and energy conversion efficiency characteristics of ionic wind generator in a multistage configuration," *J. Electrostatics*, vol. 68, pp. 36–41, Feb. 2009.

[14] R. Sigmond and I. Lågstad, "Mass and species transport in corona discharges," *High Temperature Chem. Process.*, vol. 2, no. 4, p. 5, 1993.

[15] R. S. Sigmond, "Simple approximate treatment of unipolar space-charge-dominated coronas: The Warburg law and the saturation current," *J. Appl. Phys.*, vol. 53, pp. 891–898, Feb. 1982.

[16] E. Moreau and G. Touchard, "Enhancing the mechanical efficiency of electric wind in corona discharges," *J. Electrostatics*, vol. 66, pp. 39–44, Jan. 2008.

[17] M. S. June, J. Kribs, and K. M. Lyons, "Measuring efficiency of positive and negative ionic wind devices for comparison to fans and blowers," *J. Electrostatics*, vol. 69, pp. 345–350, Aug. 2011.

[18] H. Nakamura and R. Ohyama, "An image analysis of positive ionic wind velocity under the DC corona discharge in needle-cylinder electrode system," in *Proc. IEEE Conf. Electr. Insul. Dielectr. Phenomena (CEIDP)*, Oct. 2009, pp. 192–195.

[19] E. Moreau, "Airflow control by non-thermal plasma actuators," *J. Phys. D, Appl. Phys.*, vol. 40, p. 605, Jan. 2007.

[20] R. T. Waters and W. B. Stark, "Characteristics of the stabilized glow discharge in air," *J. Phys. D, Appl. Phys.*, vol. 8, no. 4, p. 416, 1975.

[21] P. Cooperman, "A theory for space-charge-limited currents with application to electrical precipitation," *Trans. Amer. Inst. Elect. Eng. I, Commun. Electron.*, vol. 79, no. 1, pp. 47–50, Mar. 1960.

[22] V. A. Mohnen, "Formation, nature, and mobility of ions of atmospheric importance," in *Electrical Processes in Atmospheres*. Heidelberg, Germany: Springer, 1976, pp. 1–17.

[23] K. Aplin, "Aspirated capacitor measurements of air conductivity and ion mobility spectra," *Rev. Sci. Instrum.*, vol. 76, p. 104501, Jul. 2005.

[24] K. Yanallah and F. Pontiga, "A semi-analytical stationary model of a point-to-plane corona discharge," *Plasma Sour. Sci. Technol.*, vol. 21, no. 4, p. 045007, 2012.

[25] K. Yanallah, F. Pontiga, and J. H. Chen, "A semi-analytical study of positive corona discharge in wire–plane electrode configuration," *J. Phys. D, Appl. Phys.*, vol. 46, no. 34, p. 345202, 2013.
[26] W. Deutsch, "Über die dichteverteilung unipolarer ionenströme," *Ann. Phys.*, vol. 408, no. 5, pp. 588–612, 1933.
[27] R. S. Sigmond, "The unipolar corona space charge flow problem," *J. Electrostatics*, vol. 18, no. 3, pp. 249–272, 1986.
[28] J. Kuffel, E. Kuffel, and W. Zaengl, *High Voltage Engineering Fundamentals*. Oxford, U.K.: Newnes, 2000.
[29] Y. K. Stishkov and V. Chirkov, "Computer simulation of EHD flows in a needle-plane electrode system," *Tech. Phys.*, vol. 53, pp. 1407–1413, Nov. 2008.
[30] M. Goldman, A. Goldman, and R. S. Sigmond, "The corona discharge, its properties and specific uses," *Pure Appl. Chem.*, vol. 57, no. 9, pp. 1353–1362, 1985.

Emmanouil D. Fylladitakis received the B.Sc. degree in electrical energy engineering from the Technological Educational Institute (TEI) of Athens, Athens, Greece, in 2010, an M.Sc. (with distinction) degree in energy from the Heriot-Watt University, Edinburgh, Scotland, in 2012, where he received a prize for outstanding merit, and a Ph.D. degree in electronics and computer engineering department from Brunel University London, U.K, in 2016.

He is currently an External Research Associate with Brunel University London and the TEI of Athens. His current research interests include the study of corona discharges, electrohydrodynamic effects, renewable energy systems, energy storage and conservation, engineering education and distance learning systems.

Antonios X. Moronis was born in Athens, Greece, in 1967. He received the Diploma degree in electrical engineering from the Aristotle University of Thessaloniki, Thessaloniki, Greece, in 1990, and the Ph.D. degree in electrical engineering from the National Technical University of Athens, in 1995.

From 2001 to 2006, he was Assistant Professor with the Energy Engineering Department of Technological Educational Institute, Athens, Greece. He is currently an Associate Professor with the same Department and Director of the Electrotechnology and Measuring Systems laboratory. He has authored more than 45 articles in scientific journals and conference proceedings. His current research interests include dielectrics and electrical insulation, electrohydrodynamics, high-voltage applications, earthing systems in electrical installations, and fault diagnosis and predictive maintenance of electric power system components.

Dr. Moronis is a member of the Technical Chamber of Greece.

Michael P. Theodoridis received the B.Sc. degree in energy engineering from the Technological Educational Institute (TEI) of Athens, Athens, Greece, in 2000, the M.Sc. degree in power electronics and drives jointly from the University of Birmingham, Birmingham, U.K., and the University of Nottingham, Nottingham, U.K., in 2002, and the Ph.D. degree in electrical engineering from the University of Birmingham, in 2005.

From 2000 to 2001, he was at Olympic Airways, Athens, Greece. From 2005 to 2011, he was with the Department of Energy Technology, TEI of Athens. He is currently with Brunel University London, U.K. His current research interests include high-frequency converters, electrical machines and drives, and renewable energy.